Proceedings of the 2012 IEEE
International Conference on Robotics and Biomimetics
December 11-14, 2012, Guangzhou, China

An Omnidirectional Mobile Robot: Concept and Analysis

Shugen Ma, Chao Ren and Changlong Ye

Abstract— **This paper presents a novel omnidirectional wheel mechanism, referred to as MY wheel-II, based on a sliced ball structure. The wheel consists of two balls of equal diameter on a common shaft and both balls are sliced into four spherical crowns. The two sets of spherical crowns are mounted at 45° from each other to produce a combined circular profile. Compared with previous MY wheel mechanism, this improved wheel mechanism not only is more insensitive to fragments and irregularities on the floor but also has a higher payload capacity. A kinematic model of a three-wheeled prototype platform is also derived, and the problem of wheel angular velocity fluctuations caused by the specific mechanical structure is studied. The optimal scale factor (OSF) leading to a minimum of trajectory error is adopted to solve this problem. The factors influencing the OSF are investigated through simulation. In addition, the methods used for determining the OSF are discussed briefly.**

I. INTRODUCTION

In the past few years, omnidirectional mobile robots (OMRs) have received growing attention in the field of wheeled mobile robots because of their high maneuverability. Compared with non-holonomic mobile robots, OMRs, which are holonomic, are able to achieve translational and rational motions independently and simultaneously. As a result, they are extremely useful in tight environments, such as hospitals, warehouses, residential homes, and sheltered workshops for disabled people.

A variety of omnidirectional wheel mechanisms have been proposed over the past few decades. Several mechanisms based on the "universal wheel concept" have been designed, which is an assembly providing a combination of constrained and unconstrained motion when turning [1]. The initial universal wheel design was used to accomplish omnidirectional motions without changing the direction of the wheels, but this wheel type suffers from successive shocks when the individual rollers make contact with ground. The Mecanum wheel [2], Swedish wheel [3] and Alternate wheel [4], [5], [6] were proposed to remedy the gap between the rollers. Wada and Asada [7], [8] proposed a variable footprint mechanism based on a ball wheel structure and applied it to wheel chairs, but the wheel mechanism was complex. Tadakuma *et al.* [9] proposed an "Omniball" mechanism to realize high step-climbing capability. However, the mechanism has a low load carrying capability because of the mechanical structure. Pin and Killough [10] presented "orthogonal-wheels" concept and two major wheel assemblies: the longitudinal orthogonal-wheel assembly and lateral orthogonal-wheel assembly. In our previous work, we proposed a novel omnidirectional wheel mechanism, referred to as MY wheel, which is based on sliced ball structure [11]. This wheel structure is insensitive to dirt and fragments on the floor in comparison with conventional omnidirectional wheels, such as Mecanum wheel and Swedish wheel.

However, when an omnidirectional mobile platform, based on either longitudinal orthogonal-wheel assemblies or MY wheel assemblies, moves with rotation, it suffers from the problem of motor speed fluctuation. This is due to the varying contact distance from the contact point to the center of the robot platform. Mourioux *et al.* [12] analyzed the two major orthogonal wheel assemblies and proposed a control method for the longitudinal one to compensate the trajectory errors produced by using a medium contact distance in the kinematic equation. Ye *et al.* [13] proposed use of OSF instead of the medium contact distance to reduce the trajectory errors, but analyzed only a few factors that influence the OSF.

In this paper, an improved omnidirectional wheel mechanism, referred to as MY wheel-II, has been proposed. A prototype platform with three MY wheel-II assemblies has been developed, and the factors influencing the OSF are analyzed. In Section II, the MY wheel-II mechanism and the prototype platform are discussed. The use of a kinematic model of the prototype platform for the study of the problem of wheel angular velocity fluctuations is presented in Section III. In Section IV, the factors influencing the OSF, including the motor servo system, are investigated by simulation. In addition, the methods used for determining the OSF are briefly compared. Finally, conclusions are drawn in Section V.

II. MECHANISM

A. MY Wheel-II Mechanism

Fig. 1 shows the basic structure of the MY wheel-II mechanism. The wheel consists of two balls of equal diameter on a common shaft and both balls are sliced into four spherical crowns. Each spherical crown can rotate freely around its axis. The two sets of spherical crowns are mounted at 45° from each other to produce a combined circular profile. In the direction perpendicular to the shaft, the wheel has a constrained motion controlled by rotation of the main shaft, while the motion component in the direction parallel to the shaft is unconstrained. During the rotation of the main shaft, the two sets of crowns make alternative contact with the ground to realize continuous motion on the ground. The contact point of switches to from one to the other whenever the shaft turns 45°, and therefore eight switches occur during

S. Ma is with Department of Robotics, Ritsumeikan University, 525-8577, Shiga, Japan shugen@se.ritsumei.ac.jp
C. Ren is with Department of Robotics, Ritsumeikan University, 525-8577, Shiga, Japan gr0119vp@ed.ritsumei.ac.jp
C. Ye is with Department of Mechatronics Engineering, Shenyang Aerospace University, 110136, Shenyang, China clye@sia.cn

978-1-4673-2127-3/12/$31.00 © 2012 IEEE

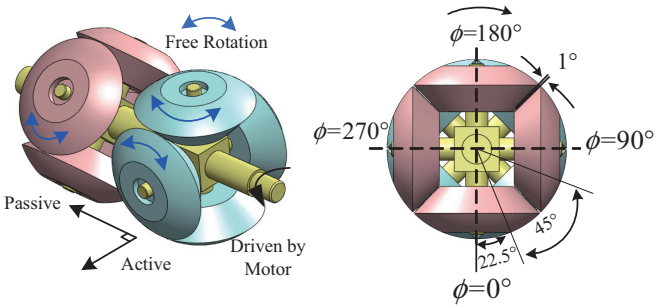

(a) (b)

Fig. 1. MY wheel-II mechanism: (a) motion principle. (b) end-view.

TABLE I
SPECIFICATIONS OF THE PROTOTYPE PLATFORM

Body Dimension	620 mm × 190 mm
Weight	40 Kg
Payload	150 Kg
DC Motor	Maxon DC Motor 90 W × 3
Radius of Wheel	60 mm
Contact Radius	D_1=147 mm, D_2=236 mm

each turn. A 1° gap exists between two adjacent spherical crowns (shown in Fig. 1(b)). Compared with other omnidirectional wheel structures, this wheel mechanism is relatively simple and stable, and has a higher payload carrying ability.

The previous MY wheel may get stuck by surface irregularities due to the specific wheel structure, i.e., the gaps between each two adjacent crowns are relatively large. In comparison, the MY wheel-II structure not only has the advantages of MY wheel (e.g., insensitivity to the dirt and fragments on the floor), but also is more insensitive to the floor irregularities because the gap between two adjacent crowns is only 1°. In addition, the MY wheel-II has a higher step climbing capability (average of 20mm height with a 60mm radius of the wheel).

B. Prototype

A CAD image of the MY wheel-II assembly is shown in Fig. 2(a). One end of the shaft is connected to the DC motor through a synchronous belt. An absolute encoder is applied to detect the switch time of contact point and a pair of spur gears is adopted to transmit the wheel rotation to the absolute encoder. To produce a prototype platform with three full degrees of freedom, three MY wheel-II assemblies are arranged with a 120° interval angle underneath the steel disk (Fig. 2(b)). Although the contact point of each module switches from one wheel to the other, the robot has only three contact points at any moment. The specifications of the prototype platform are listed in Table I.

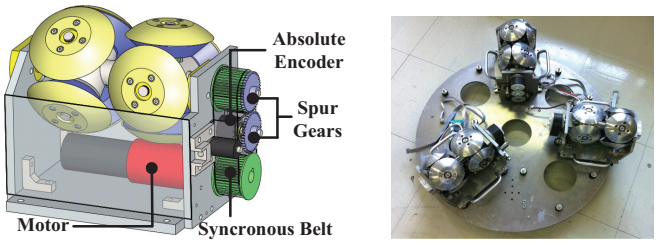

(a) (b)

Fig. 2. (a) CAD model of MY Wheel-II assembly. (b) prototype platform.

III. KINEMATIC MODELING AND MOVEMENT SIMULATIONS

A. Kinematic Modeling

Fig. 3 presents the geometrical model of our robot prototype with definitions of the variables necessary for developing the kinematic model. The world coordinate frame is $\{O_w\}$ and the moving coordinate frame is $\{O_m\}$ that is assumed to be fixed on the center of gravity (c.g.) of the robot. θ denotes the angle between X_w- and X_m- frame, i.e., the rotational angle of the moving coordinate frame with respect to the world coordinate frame. $\dot{\Phi} = \begin{bmatrix} \dot{\phi}_1 & \dot{\phi}_2 & \dot{\phi}_3 \end{bmatrix}^T$ is the wheel angular velocity vector. $\mathbf{T_i}$ $(i = 1,2,3)$ gives the driven direction of each wheel in the moving coordinate frame. D_1 and D_2 are the distance from the c.g. of the robot to the inner and outer contact point in each wheel respectively. R is the radius of the wheel. The posture vector of the c.g. of the robot in the world coordinate frame is specified as $\mathbf{q} = \begin{bmatrix} x & y & \theta \end{bmatrix}^T$. The robot velocity expressed in the moving coordinate is $\mathbf{V} = \begin{bmatrix} V_x & V_y \end{bmatrix}$.

The coordinate transformation matrix from the moving coordinate frame to the world coordinate frame is given by:

$$ {}^{w}_{m}\mathbf{R} = \begin{bmatrix} \cos\theta & -\sin\theta & 0 \\ \sin\theta & \cos\theta & 0 \\ 0 & 0 & 1 \end{bmatrix} \tag{1} $$

Then we have:

$$ \dot{\mathbf{q}} = {}^{w}_{m}\mathbf{R} \begin{bmatrix} V_x \\ V_y \\ \dot{\theta} \end{bmatrix} \tag{2} $$

The kinematic relationship in the moving coordinate can be described as follows[10][14]:

$$ \begin{aligned} R\dot{\phi}_1 &= -\tfrac{1}{2}V_x + \tfrac{\sqrt{3}}{2}V_y + L_1\dot{\theta} \\ R\dot{\phi}_2 &= -\tfrac{1}{2}V_x - \tfrac{\sqrt{3}}{2}V_y + L_2\dot{\theta} \\ R\dot{\phi}_3 &= V_x + L_3\dot{\theta} \end{aligned} \tag{3} $$

where L_i $(i = 1,2,3)$ represents the distance between the c.g. of the robot and the contact point with ground of each wheel (Fig. 3) and is given as:

$$ L_i = \begin{cases} D_1, if -\frac{\pi}{8} + \frac{n\pi}{2} < \phi_i < \frac{\pi}{8} + \frac{n\pi}{2} \\ D_2, if \ \frac{3\pi}{8} + \frac{n\pi}{2} < \phi_i < \frac{5\pi}{8} + \frac{n\pi}{2} \end{cases} \quad n = 0, \pm 1, \pm 2 \ldots $$

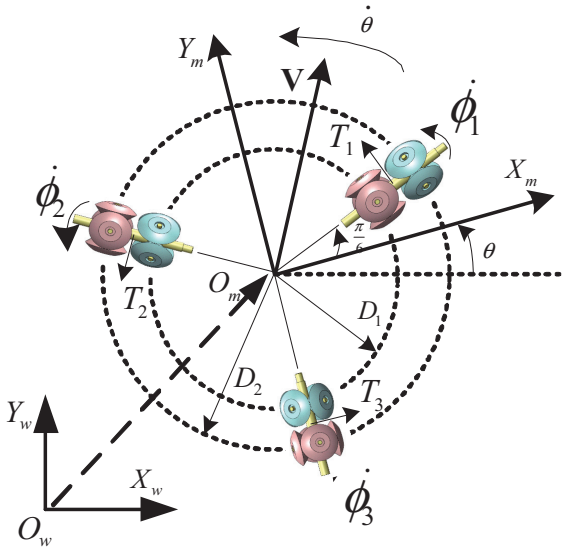

Fig. 3. Model of three-wheeled omnidirectional mobile robot

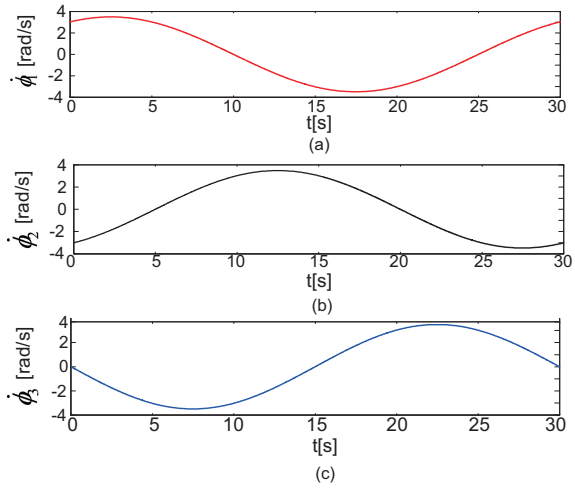

Fig. 4. Wheel angular velocities of robot translational motion. (a) angular velocity of wheel 1. (b) angular velocity of wheel 2. (c) angular velocity of wheel 3.

where ϕ_i is the angle of wheel i.

Combining (2) and (3), the inverse kinematic equation of a three-wheeled omnidirectional mobile robot in the world coordinate can be expressed as follows:

$$\dot{\Phi} = \frac{1}{R}\mathbf{J}^{-1}\dot{\mathbf{q}} \tag{4}$$

where $\mathbf{J}^{-1} \in \Re^{3\times 3}$ matrix is given by:

$$\mathbf{J}^{-1} = \begin{bmatrix} -\cos(\frac{\pi}{3}-\theta) & \cos(\frac{\pi}{6}+\theta) & L_1 \\ -\sin(\frac{\pi}{6}-\theta) & -\cos(\frac{\pi}{6}-\theta) & L_2 \\ \cos\theta & \sin\theta & L_3 \end{bmatrix}$$

Then, the robot velocity vector $\dot{\mathbf{q}}$ can be expressed as

$$\dot{\mathbf{q}} = R\mathbf{J}\dot{\Phi} \tag{5}$$

where $\mathbf{J}$ corresponds to the Jacobian matrix relating the wheel velocity vector to the robot velocity vector.

B. Movement Simulations

Assuming that the translational reference trajectory is a circle and the robot rotational reference velocity $\dot{\theta}$ is constant, the reference translational and rotational trajectory can be obtained as follows:

$$\begin{cases} x_{wd} = r\cos\omega t \\ y_{wd} = r\sin\omega t \\ \theta_d = \dot{\theta}_d t \end{cases} \tag{6}$$

where r is the radius of the reference circle, ω is the angular velocity of the translational movement. $\mathbf{q}_d = \begin{bmatrix} x_{wd} & y_{wd} & \theta_d \end{bmatrix}^T$ is the desired posture vector in the world coordinate frame.

As can be seen from (4), we can easily deduce that the changes of L_i (i.e., the switches of contact distance) have no influence on the wheel angular velocity $\dot{\phi}_i$ when $\dot{\theta}_d$ is 0. In other words, there are no velocity fluctuations for translational motion of the robot. This is because the two sets of crowns in each wheel move at the same velocity and have identical trajectories on the ground. Fig. 4 shows the wheel angular velocities when the reference trajectory parameters are set as: $r = 1\,m$, $\omega = \pi/15\,rad/s$ and $\dot{\theta}_d = 0$.

Nevertheless, if the robot performs translational and rotational motions simultaneously, the wheel angular velocity will fluctuate because of the varying contact distance L_i. For further analysis, we set the parameters for reference trajectory I and II as follows:

Reference trajectory I:

$r = 1\,m$, $\omega = \pi/15\,rad/s$, and $\dot{\theta}_d = \pi/15\,rad/s$.

Reference trajectory II:

$r = 1\,m$, $\omega = \pi/15\,rad/s$, and $\dot{\theta}_d = 2\pi/15\,rad/s$.

The wheel angular velocities for reference trajectory I and II are shown in Fig. 5 (solid line) and Fig. 6 (solid line), respectively. We can see that significant fluctuations of the wheel angular velocities exist when the robot moves with rotation. In addition, the fluctuations will be much more severe if reference translational velocity or rotational velocity increases; it is impossible for the motor servo system to track the wheel angular velocity command because of its limited bandwidth.

Furthermore, for the circular reference trajectory, it is worth noting that the wheel angular velocities are square waves only when $\omega = \dot{\theta}_d$. Otherwise, the wheel angular velocities are the superposition of sinusoidal and square wave, which can be obtained by solving (4).

IV. ANALYSIS OF THE OPTIMAL SCALE FACTOR

One solution to the problem of wheel angular velocity fluctuations is to use a constant L instead of the real varying L_i in (4). That is, the desired wheel angular velocity is calculated by (4) with a constant L, and therefore, the obtained wheel angular velocity will be smooth. In this case, the robot moves as if only one point contacts with ground for each module, but trajectory errors will be produced accordingly. We set $L = D_1 + \gamma(D_2 - D_1)$, while γ is the scale

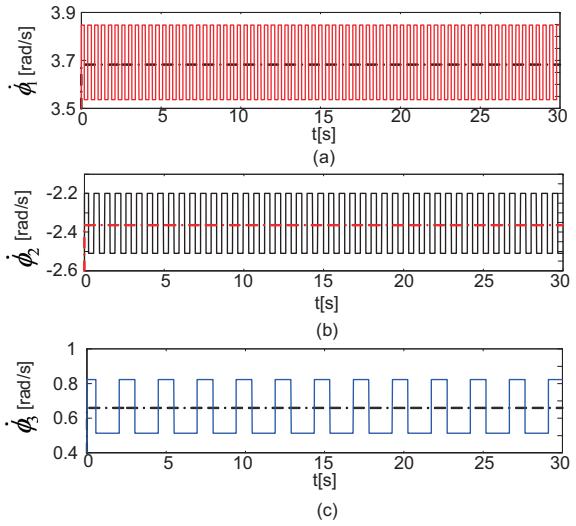

Fig. 5. Wheel angular velocity for reference trajectory I. (a) angular velocity of wheel 1. (b) angular velocity of wheel 2. (c) angular velocity of wheel 3.

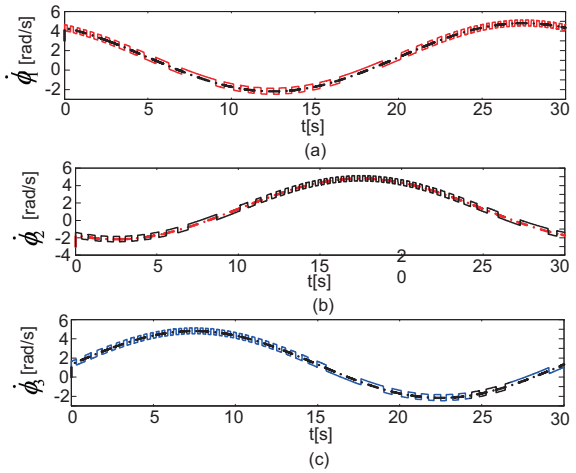

Fig. 6. Wheel angular velocity for reference trajectory II. (a) angular velocity of wheel 1. (b) angular velocity of wheel 2. (c) angular velocity of wheel 3.

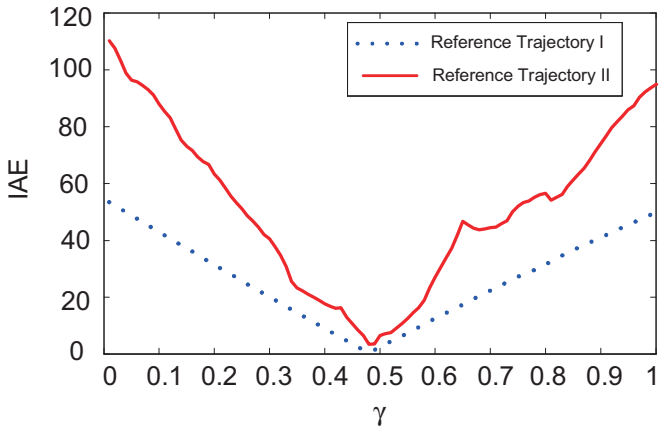

Fig. 7. IAE versus γ for reference trajectory I and II.

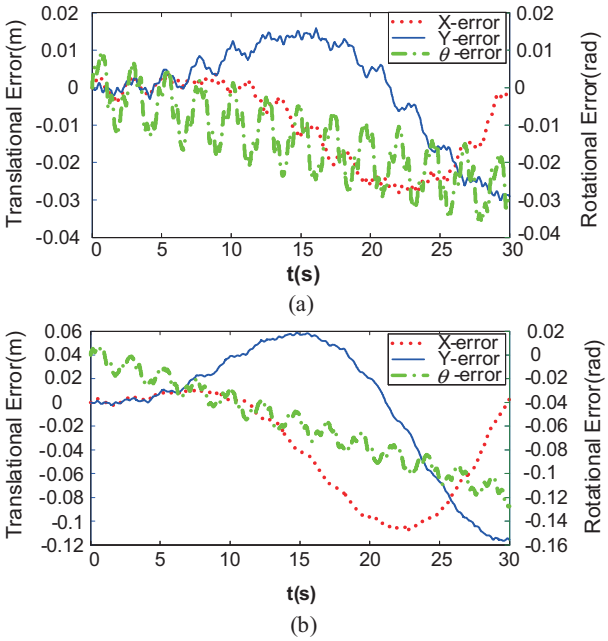

Fig. 8. Trajectory errors with different γ. (a) trajectory errors with $\gamma = 0.47$. (b) trajectory errors with $\gamma = 0.5$.

factor to be determined. The scale factor γ was selected as 0.5 to obtain smooth wheel angular velocities in [12]. In [13], the OSF that leads to the minimum trajectory errors was proposed, but only a few factors that influence the OSF were discussed and the motor servo system was ignored. In this section, all factors influencing the OSF, including the motor servo system, are discussed along with the methods used to determine the OSF.

A. Motor Servo System

We assume that the response of the motor servo system has no overshoot in order to facilitate the analysis. The response process of a servo system with no overshoot is similar to that of the first-order inertia element. Considering that our purpose is merely to analyze the influence of the motor servo system on the OSF, for the sake of simplicity, we use the first order inertia element to simulate the motor servo system. The first-order inertia element:

$$\frac{1}{Ts+1} \tag{7}$$

As known from control theory, the transient time for the first-order inertia element is $3T \sim 4T$. Besides, it was assumed that the gear ratio of the motor is 1.

B. Optimal Scale Factor

Because we chose a constant value of $L = D_1 + \gamma(D_2 - D_1)$ instead of the real one for the inverse kinematic equation (4), trajectory errors will be correspondingly introduced (for a detailed discussion, see [13]). Here the integrated absolute error (IAE) was used as the error evaluation criteria:

$$IAE = \int \left(|e_x| + |e_y| + |e_\theta|\right) dt \tag{8}$$

$$e_x = \int (\dot{x}_d - \dot{x})dt = \int \left\{ -r\omega[\sin\omega t - \sin(\omega t - \theta_d + \theta)] - \frac{(L_1 + L_2 - 2L_3)\cos\theta - \sqrt{3}(L_2 - L_1)\sin\theta}{L_1 + L_2 + L_3} D\dot{\theta}_d \right\} dt \quad (11)$$

$$e_y = \int (\dot{y}_d - \dot{y})dt = \int \left\{ r\omega[\cos\omega t - \cos(\omega t - \theta_d + \theta)] - \frac{(L_1 + L_2 - 2L_3)\sin\theta - \sqrt{3}(L_2 - L_1)\cos\theta}{L_1 + L_2 + L_3} D\dot{\theta}_d \right\} dt \quad (12)$$

$$e_\theta = \int (\dot{\theta}_d - \dot{\theta})dt = \int \left[\left(1 - \frac{3}{L_1 + L_2 + L_3} D \right) \dot{\theta}_d \right] dt \quad (13)$$

where $\theta = \frac{3}{L_1+L_2+L_3}[(D_1 + \gamma(D_2 - D_1)]\dot{\theta}_d$, and $D = D_1 + \gamma(D_2 - D_1)$.

Fig. 7 shows the relationship between IAE and the scale factor γ for the reference trajectory I and II defined in the previous section. Both the optimal scale factors are 0.47. The dot dash lines in Fig. 5 and Fig. 6 represent the wheel angular velocities calculated in (4) using the optimal γ for reference trajectory I and II. To demonstrate the effectiveness of OSF, reference trajectory I was taken as an example. We plotted the trajectory errors for reference trajectory I using $\gamma = 0.47$ (Fig. 8a) and $\gamma = 0.5$ (Fig. 8b), respectively. It is obvious that the trajectory errors are reduced significantly by using optimal γ (i.e., 0.47) than that of 0.5. In the above simulations, the initial wheel positions $(\phi_{10}, \phi_{20}, \phi_{30})$ and initial robot orientation θ_0 were set as 0 rad, and the parameter T for the servo system was set as 0.1 s.

C. Factors Influencing the Optimal Scale Factor

To investigate the influences on the OSF, the expressions of trajectory errors (11)-(13) were obtained according to (4)-(6). As can be seen in (11)-(13), the parameters that possibly effect the OSF can be classified as follows:

Mechanical parameters: D_1 $[m]$, D_2 $[m]$.
Trajectory parameters: r $[m]$, ω $[rad/s]$, $\dot{\theta}$ $[rad/s]$.
Initial wheel positions: $(\phi_{10}, \phi_{20}, \phi_{30})$ $[rad]$.
Initial robot orientation: θ_0 $[rad]$.
Motor servo system: T $[s]$.

In the following simulations, each parameter was selected as a variable while keeping the other parameters constant to investigate the influence of that parameter on the optimal γ. The values of the above parameters, except the one regarded as variable, were set as follows: $D_1 = 0.147\,m, D_2 = 0.236\,m$, $r = 1\,m$, $\omega = \pi/5\ rad/s$, $\dot{\theta}_d = \pi/10\ rad/s$, $\theta_0 = 0\,rad$, $\phi_{10} = \phi_{20} = \phi_{30} = 0\,rad$, $T = 0.1\,s$. The influence of each parameter shown above on the OSF has been listed in Table II-Table III. From these results, it can be conclude that all the parameters involved in (11)-(13) influence the OSF. The following should be noted:

1. The wheel radius R is not included in the trajectory error expressions (11)-(13). Hence, it not only has no influence on the OSF, but also has no relationship with the trajectory errors.
2. Although parameters for initial wheel positions, initial robot orientation and the motor servo system are not involved in (11)-(13), they influence the values of some elements in the trajectory error expressions which are $(L_1 + L_2 + L_3)$, $(L_1 + L_2 - 2L_3)$ and $(L_2 - L_1)$. Consequently, they influence the OSF.

TABLE II
PARAMETERS INFLUENCES

D_1 $[m]$	0.1	0.2	0.3	0.4	0.5	0.6
OSF	0.52	0.57	0.58	0.58	0.6	0.65
D_2 $[m]$	0.197	0.247	0.297	0.347	0.397	0.447
OSF	0.53	0.5	0.5	0.5	0.47	0.43
r $[m]$	0.1	0.3	0.5	0.7	0.9	1
OSF	0.61	0.50	0.44	0.48	0.47	0.48
ω $[rad/s]$	$2\pi/5$	$\pi/5$	$\pi/8$	$\pi/10$	$\pi/12$	$\pi/15$
OSF	0.61	0.5	0.44	0.48	0.47	0.48
$\dot{\theta}_d$ $[rad/s]$	$2\pi/5$	$\pi/5$	$\pi/8$	$\pi/10$	$\pi/12$	$\pi/15$
OSF	0.48	0.49	0.51	0.5	0.5	0.54
θ_0 $[rad]$	$\pi/8$	$\pi/6$	$\pi/4$	$\pi/2$	π	$\pi/2$
OSF	0.53	0.55	0.55	0.54	0.55	0.56
T $[s]$	0.034	0.1	0.17	0.23	0.3	0.33
OSF	0.5	0.53	0.55	0.57	0.58	0.62

TABLE III
INFLUENCE OF PARAMETER $(\phi_{10}, \phi_{20}, \phi_{30})$

$(\phi_{10}, \phi_{20}, \phi_{30})$ $[rad]$	0,0,0	0.3,1.5,0.8	1.6,2.6,3.1	2.2,1.9,0.8	0.5,0.3,2.7
OSF	0.5	0.46	0.52	0.48	0.49

For one robot prototype, the mechanical parameters will be determined. Also, the motor servo system can be assumed to be constant. However, the trajectory parameters and initial wheel positions, and initial wheel orientation will make the OSF unapplicable in the real practice. Therefore, one work in the future is to investigate the influences of these three aspects.

D. Methods for Determining the Optimal Scale Factor

It is worthy pointing out that the relationship between IAE and scale factor γ is not always a unimodal function, but sometimes it can be multimodal (e.g., the relationship between IAE and γ for reference trajectory II shown in Fig. 7).

As high accuracy of optimal γ is not necessary in practice,

the method of exhaustion is preferred to determining the OSF from the computational cost aspect. If the precision to two decimal places is required, the simulation times are 100 using the method of exhaustion. In comparison, when optimization methods are selected, the global optimization methods must be used to guarantee the reliable results due to the fact that relationship between IAE and γ may not always be unimodal. However, the problem of heavy computation is introduced with the global optimization methods as compared to exhaustion method. Take genetic algorithm (GA) as an example; if the population is chosen to be 80 [15] and the final generation is 60, and 4800 simulation times are necessary, which is much larger than that required for the method of exhaustion. Consequently, the method of exhaustion was selected for determining the OSF in the above simulations.

V. CONCLUSIONS AND FUTURE WORKS

In this paper, we proposed a novel omnidirectional wheel mechanism, referred to as MY wheel-II, based on a sliced ball structure. This improved wheel structure is superior to the previously proposed MY wheel structure because it is more insensitive to the floor fragments and irregularities, and has a higher payload capacity. A kinematic model for a developed platform with three MY wheel-II assemblies was built and the problem of wheel angular velocity fluctuations is studied. When the robot moves with rotation, the fluctuations are produced by the varying contact distance in each wheel with respect to the center of the prototype platform. To address this problem, the OSF was adopted to obtain smooth wheel angular velocities, at the same time producing minimum trajectory errors. In addition, the factors influencing the OSF are investigated, which can be classified as: mechanical specifications, reference trajectory, initial wheel positions, initial robot orientation and motor servo system. Finally, the methods used to determining the OSF were discussed briefly, and the method of exhaustion is preferred because of its lower computation requirements.

In the future, certain influencing factors such as initial wheel position and initial orientation will be analyzed to make the OSF applicable in practice.

VI. ACKNOWLEDGMENTS

The authors are deeply grateful to Huang Yan for his design of the wheel mechanism and prototype and to Lin Lin for his design of the motor control system.

REFERENCES

[1] P. F. Muir and C. P. Neuman, "Kinematic modeling of wheeled mobile robots," *Journal of Robotic Systems*, vol. 4, no. 2, pp. 281–340, 1987.

[2] B. Ilou, "Wheels for a course stable self-propelling vehicle movable in any desired direction on the ground or some other base," USA Patent, 1975.

[3] G. Indiveri, "Swedish wheeled omnidirectional mobile robots: Kinematics analysis and control," *IEEE Transactions on Robotics*, vol. 25, no. 1, pp. 164 –171, Feb. 2009.

[4] K.-S. Byun and J.-B. Song, "Design and construction of continuous alternate wheels for an omnidirectional mobile robot," *Journal of Robotic Systems*, vol. 20, no. 9, pp. 569–579, 2003.

[5] J.-B. Song and K.-S. Byun, "Design and control of a four-wheeled omnidirectional mobile robot with steerable omnidirectional wheels," *Journal of Robotic Systems*, vol. 21, no. 4, pp. 193–208, 2004.

[6] H. Asama, M. Sato, N. Goto, H. Kaetsu, A. Matsumoto, and I. Endo, "Mutual transportation of cooperative mobile robots using forklift mechanisms," in *Proceeding of IEEE International Conference on Robotics and Automation*, vol. 2, Apr. 1996, pp. 1754 –1759.

[7] M. West and H. Asada, "Design and control of ball wheel omnidirectional vehicles," in *Proceedings of IEEE International Conference on Robotics and Automation*, vol. 2, May 1995, pp. 1931 –1938.

[8] M. Wada and H. Asada, "Design and control of a variable footprint mechanism for holonomic omnidirectional vehicles and its application to wheelchairs," *IEEE Transactions on Robotics and Automation*, vol. 15, no. 6, pp. 978 –989, Dec. 1999.

[9] K. Tadakuma and R. Tadakuma, "Mechanical design of "omni-ball": Spherical wheel for holonomic omnidirectional motion," in *Automation Science and Engineering, 2007. CASE 2007. IEEE International Conference on*, Sept. 2007, pp. 788 –794.

[10] F. Pin and S. Killough, "A new family of omnidirectional and holonomic wheeled platforms for mobile robots," *IEEE Transactions on Robotics and Automation*, vol. 10, no. 4, pp. 480 –489, Aug 1994.

[11] C. Ye and S. Ma, "Development of an omnidirectional mobile platform," in *Proceeding of IEEE International Conference on Mechatronics and Automation*, Aug. 2009, pp. 1111 –1115.

[12] G. Mourioux, C. Novales, G. Poisson, and P. Vieyres, "Omnidirectional robot with spherical orthogonal wheels: concepts and analyses," in *Proceedings IEEE International Conference on Robotics and Automation*, May 2006, pp. 3374 –3379.

[13] C. Ye, H. Li, and S. Ma, "Kinematic analysis of an omnidirectional mobile robot with my wheels," in *2011 IEEE International Conference on Robotics and Biomimetics (ROBIO)*, Dec. 2011, pp. 1748 –1753.

[14] K. Watanabe, Y. Shiraishi, S. Tzafestas, J. Tang, and T. Fukuda, "Feedback control of an omnidirectional autonomous platform for mobile service robots," *Journal of Intelligent and Robotic Systems*, vol. 22, pp. 315–330, 1998.

[15] J. Grefenstette, "Optimization of control parameters for genetic algorithms," *IEEE Transactions on Systems, Man and Cybernetics*, vol. 16, no. 1, pp. 122 –128, Jan. 1986.